

# SCOPING OF AN AIR SUPPLY CONFIGURATION FOR ACTIVE FLOW **CONTROL ON A COMMERCIAL TRANSPORT AIRPLANE HIGH-LIFT** SYSTEM

C.P. van Dam<sup>1</sup>, Seyedeh Sheida Hosseini<sup>2</sup>, Shishir A. Pandya<sup>2</sup>

<sup>1</sup>University of California - Davis, Davis, CA 95616, USA <sup>2</sup>NASA Ames Research Center, Moffett Field, CA 94035, USA

#### **Abstract**

A scoping study is being conducted on the air supply for a microjet-based active flow control (AFC) system on a twin-turbofan commercial transport airplane. Microjets provide circulation control using small surface-normal pneumatic jets located near the trailing edge of a lifting surface such as a wing or flap. When located on the pressure side of the lifting surface they increase the lift, and when located on the suction side they decrease lift. In this study, microjets are considered for installation in the flaps of the high-lift version of the Common Research Model (CRM-HL). Two different architectures to supply the air for the microjets are considered: (1) bleed air from the airplane's auxiliary power unit (APU) plus ram air, and (2) engine fan bleed air plus ram air. A model based on the 1D compressible flow equations is applied to analyze the air supply system architectures and predict the microjet flow rate with the resulting airplane performance changes based on Reynolds-averaged Navier-Stokes modeling of microjets on the CRM-HL. The results of this scoping study are encouraging in that pressurized air from the APU or the engine fan can be used to entrain ram air and thereby increase the AFC mass flow rate to achieve effective lift control and airplane performance enhancement during takeoff and landing.

Keywords: Takeoff, Landing, Flap, Climb Gradient, Lift-to-Drag Ratio

## 1. Nomenclature

Wing aspect ratio =  $b^2/S$ AR

b Wing span

c Wing mean aerodynamic chord

Airplane drag coefficient =  $\frac{D}{q_{\infty}S}$  $C_D$ 

Airplane lift coefficient =  $\frac{L}{q_{\infty}S}$  $C_L$ 

Pressure coefficient =  $\frac{p-p_{\infty}}{q_{\infty}}$  $C_p$ 

Mass flow coefficient =  $\frac{m_j}{\rho_{\infty}V_{\infty}}$ Momentum coefficient =  $\frac{\dot{m}_j}{a}$  $C_q$ 

 $C_{\mathfrak{u}}$ 

Diameter air supply duct d L/D Airplane lift-to-drag ratio

Mach number Μ Air mass flow rate ṁ Total pressure  $p_t$ 

Freestream dynamic pressure =  $\frac{\rho_{\infty}V_{\infty}^2}{2}$ q∞

#### Scoping of an AFC Air Supply Configuration

Re Airplane Reynolds number =  $\frac{\rho_{\infty} V_{\infty} \bar{c}}{\mu}$ 

T/W Airplane thrust-to-weight ratio

T<sub>t</sub> Total temperature S Reference wing area

v Flow velocity

V<sub>jet</sub> Average microjet exit velocity

V<sub>LOF</sub> Airplane lift-off speed

V<sub>MU</sub> Airplane minimum unstick speed

V<sub>R</sub> Airplane rotation speed

V<sub>REF</sub> Airplane reference landing speed

V<sub>SR</sub> Airplane 1-g stall speed

V<sub>2</sub> Airplane take-off safety speed

V<sub>∞</sub> Freestream velocityw Air weight flow rateα Angle of attack

η<sub>i</sub> Isentropic efficiency of subsonic nozzle

μ Absolute viscosity

ρ Air density

Subscript:

a APU air
f Fan air
j Jet
jet Microjet
max Maximum
r Ram air
∞ Freestream
1,2,..,6 Station number

### 2. Introduction

High-lift systems are critical for the safe and efficient operation of commercial transport airplanes with the design of these systems being complex as explained by Flaig & Hilbig [1], Nield [2], Rudolph [3], Reckzeh [4], De Resende [5], Kafveke et al. [6], van Dam [7], and others. Important airplane performance parameters include maximum lift coefficient during takeoff and landing, lift-to-drag ratio during takeoff, and lift coefficient at the angle of attack limited by the tail clearance angle on takeoff and landing. Active flow control (AFC) is being considered to enhance one or more of these parameters and thereby improve the overall mission performance of commercial transport airplanes. Here, microjet-based AFC systems for controlling the lift and improving the aerodynamic performance of flaptype high-lift systems are being considered. Microjets are small, nominally-orthogonal jets located close to the trailing edge of the flaps used during takeoff and landing. Located near the trailing edge, microjets increase lift when active on the pressure side and decrease lift on the suction side. The combination of pressure side and suction side microjets allows for rapid modulation of the aerodynamic lift generated by the wing as well as the spanwise distribution of the lift in the high-lift configuration without additional deflection of the flaps. Effective microjet-based lift control for multi-element airfoils has been predicted using computational fluid dynamics (CFD) [8, 9, 10] and recently verified experimentally [11]. This paper builds on an earlier study focusing on the impact of a microjet-based AFC system on the lift coefficient at the angle of attack limited by the tail clearance angle on landing and the effect on the mission performance of the Common Research Model (CRM) airplane [12]. The focus of this paper is on methods of delivering the required mass flow rate and momentum of the airflow provided to the microjets during takeoff.

To obtain insights into system layouts considered in the past and related constraints encountered in the system development process, the following section presents a brief review of air-blowing AFC systems designed for flight applications. Next, the CRM airplane details plus the conceptual layout of the air supply system and the CFD-based prediction of microjet effects on the CRM lift and drag are presented. This is then followed by the methodology used to size the air supply system and

presentation and discussion of the results on the airplane performance characteristics. Finally, conclusions and recommended next steps are presented.

## 3. Review of Air Blowing-based AFC Flight Systems

A brief review is presented of actual or studies of flight applications of AFC systems involving blowing of air for flow separation mitigation and/or circulation enhancement.

Englar et al. [13] flight tested the circulation control wing (CCW) concept on an A-6 airplane with AFC air supplied through bleed extracted from the airplane's two turbojet engines with engine thrust and AFC-based lift independently variable. The flight experiment was successful with the air supply system working well and the AFC providing excellent lift enhancement and control. However, it was noted that the supply duct pressure drop predictions were found to be optimistic, requiring higher engine thrust settings than predicted. To safely manage the high bleed air temperatures, titanium components as well as thermal barriers protecting aluminum wing components were installed.

In 1994, Englar et al. [14] applied lessons learned from the A-6 CCW flight demonstrator in a study on the impact of CCW on the performance characteristics of a Boeing 737. This was a scoping study with AFC air supply system requirements addressed in some detail. Only bleed air from the fan was considered to supply the CCW on takeoff and landing with a maximum fan pressure ratio (FPR) of 1.5. This study suggests that engine fan bleed can provide the necessary flow rates and pressures for effective circulation control.

Werner-Spatz et al. [15] present a multidisciplinary conceptual design methodology and sample trade study for airplane configurations with AFC-based blown-flap high-lift systems where the tangential-blowing actuators are located at the knee of the deflected flap allowing for aerodynamic effectiveness at high deflection angles. In this study, the main goal was to increase the maximum lift coefficient during takeoff and landing and thereby, decrease the required field lengths. Engine bleed air is used to supply the AFC system with air taken from different fan and engine core stations depending on the actuator pressure requirements.

Hartwich et al. [16] focused on tangential blowing for flow separation mitigation to allow for simpler, lighter, high-lift systems requiring smaller or no flap track fairings. The AFC system integration studies were conducted for the ERA-0003, an early version of the CRM airplane configuration. Different air supply sources were considered including bleed from the auxiliary power unit (APU) on the airplane, engine fan bleed, engine core bleed, and a combination of engine core bleed and air from a dedicated APU. For the AFC concept studied, available pressure was seen as more critical than air flow rate. This also resulted in the conclusion that given the limited amount of bleed air that can be provided by the APU and engines, follow-up studies would have to address AFC effectiveness at much reduced mass flow rates.

In a follow-up study, Hartwich et al. [17] developed an initial AFC implementation involving a total of 74 tangential blowing actuators placed into the leading edges of the inboard and outboard trailing edge flaps of a CRM-HL type configuration. In this study, the focus is on greatly reducing the flow rate and pressure requirements by trading the number of actuators against pressure for a given flow rate.

The air supply system for a sweeping jet-based AFC-enabled vertical tail flight tested on the Boeing 757 ecoDemonstrator in 2015 was discussed by Mooney et al. [18], Alexander et al. [19], and Whalen et al. [20]. Given bleed air from the Boeing 757 APU was used to supply the AFC system, the maximum air flow available was 7 lb/s. Because of losses from ducting and the heat exchanger (the latter installed to ensure AFC actuator exit temperatures are below rudder structural material temperature limits), the pressure available at the AFC actuators was less than 30 psi (pressure ratio PR  $\approx$  2) which was adequate for the selected sweeping jet actuators installed to the trailing edge of the fixed portion of the vertical tail.

Bertels et al. [21] studied an AFC system involving pulsed jet actuators (PJA) integrated into the flaps of a single-aisle commercial transport for improved maximum lift during landing. The system considered includes actuators plus sensors, conduits to supply pressurized air, and a (redundant) power and communication system to provide actuator control with AFC air from engine bleed or electrical compressors. The study concludes that the introduction of the PJA system requires at least an increase

in maximum lift coefficient of 0.2 to justify the increase in system weight and required power. For a maximum lift coefficient increase of 0.4, maximum take-off weight is predicted to change by -0.3 % and operating empty weight by -0.6 %, while the total mission fuel burn remains virtually constant.

Woszidlo, Shmilovich, Vijgen, et al. [22, 23, 24, 25] studied AFC concepts on a twin-engine reference airplane, including AFC to mitigate flow separation over deflected ailerons. The reference airplane is significantly smaller than the CRM with the smaller size posing challenges regarding the AFC air conduit size and routing. The study includes an assessment of performance benefits and airplane system impact of several sources of airflow for the AFC actuators. Two air supply architectures are considered for tangential blowing to mitigate flow separation over deflected ailerons; air from the APU load compressor, and air from electrically powered air compressors. Several electric compressor layouts are studied including dedicated AFC compressors powered by generators or batteries, and a layout where air to the aileron AFC actuators is provided by the electric pumps used for cabin pressurization. The air intake for the compressors is through pitot inlets. The architecture with the air supplied by the APU is predicted to produce the smaller increase (0.09-0.13%) in the operating empty weight (OEW) of the airplane.

Cai et al. [26] conducted a detailed system-level assessment of AFC for high-lift devices on commercial transport airplanes. Their focus was on tangential blowing (sweeping jets) based AFC on a twinturbofan, 242-passenger, twin-aisle, transonic, transport airplane with three sources of AFC air considered separately or in combination: engine core bleed, APU bleed, and ram air. In this study, ram air, because of its low pressure, is pressurized using electric compressors with the required power extracted from the engines. This makes any significant use of ram air less economical. The predicted fuel savings are the result of the reduction in airplane cruise drag on account of elimination of the flap track fairings not needed for the revised (simple hinged) flap system. Note the high-lift system is only deployed during takeoff and landing and, hence, the flaps and its AFC system are not used during cruise. The predicted decline in the fuel savings with increasing AFC mass flow rate are the result of the increase in AFC system weight and, with that, the airplane's OEW.

The above air blowing-based AFC system studies provide a wealth of information on air supply system options and constraints. With regards to the design of a microjet-based AFC system, the main conclusions that can be drawn from these studies are:

- For a CRM-size airplane, a standard APU can supply an approximate maximum 8 lb/s of bleed air at a PR ≈ 4.
- A dedicated AFC APU can supply as much as 28 lb/s of air at a PR  $\approx$  5.
- Engine core bleed can be a source of high-pressure flow; but, for high bypass ratio engines, the available flow rates are limited.
- High AFC air pressure ratios result in high temperatures and this may require heat exchangers
  to cool the supplied air resulting in significant pressure losses or application of more advanced
  materials that can withstand the higher temperatures.
- Higher AFC air temperatures do result in higher jet momentum coefficients for a given mass flow coefficient [27].
- Engine fan bleed can be a source of significant mass flow rates but at modest pressures with available FPR to be more limited with increasing engine bypass ratio as indicated by Daggett et al. [28]. High mass flow rates require larger ducts making the transport of the air from the engines to the AFC actuators a challenge. Also, the FPR will be significantly reduced at lower thrust settings during approach for landing.
- Limited space in the wings for air conduits and other AFC system components is a challenge when considering AFC application on smaller sized (single-aisle) transport airplanes.
- Because of its low pressure, ram air as a sole source is impractical for AFC applications.

### 4. CRM Configuration and Performance Details

The Common Research Model (CRM) has been developed to provide a state-of-the-art, twin-engine, transonic, transport airplane configuration for computational and experimental aerodynamic analysis and be able to share the details of these studies including relevant geometric details in the public domain. The CRM cruise configuration was introduced by Vassberg et al. [29] in 2008, and Lacy & Sclafani [30] complemented this with the high-lift configuration in 2016. The latter, denoted CRM-HL,

has been used to study the impact of microjets on its high-lift performance characteristics by Hosseini et al. [31, 32]. The CRM semispan b/2 is 1156.8 in. for a wingspan b = 192.8 ft, reference wing area S = 4,130 ft<sup>2</sup>, mean aerodynamic chord  $\bar{c}$  = 275.8 in., and wing aspect ratio AR = 9.0.

The CRM-HL has been studied for a series of AIAA high-lift workshops. For the purposes of this paper, the wing/body configuration from the 3rd AIAA CFD High-Lift Prediction Workshop (HiLiftPW-3) [33] is selected, for which the slat and flaps are deployed at 30° and 37°, respectively (so-called Flap 37 configuration). This geometry does not include the nacelles, pylons, empennage, and slat & flap support brackets. NASA's OVERFLOW-2 [34] methodology was applied to solve the Reynolds-averaged Navier-Stokes equations on the structured overset computational grid. Prior work by the authors [32] has provided extensive comparisons with computational results shared at HiLiftPW-3 showing good agreement. Comparisons with wall-corrected wind tunnel results are presented in Ref. [31] and again show good agreement. For the present study, in addition to extending the  $\alpha$ -range for the Flap 37 CFD simulations to include stall, computational grids were generated and CFD solutions were obtained for four additional settings; Flap 10 (flaps at 10°, slats at 22° and 30°). Flap 25 (flaps at 25°, slats at 30°), and Flap 40 (flaps at 40°, slats at 30°). For the Flap 25 and 40 configurations, results are limited to the operational (linear) lift regime ( $\alpha = 0^{\circ}$ -10°).

In Fig. 1, the CFD predicted effect of flap setting on the lift curve of the CRM-HL is depicted. The results show little improvement in lift for Flap 40 compared to Flap 37. In addition, the change in slat angle has a minor effect on lift in the linear regime with the smaller slat angle reducing the stall angle and thereby the maximum lift coefficient.

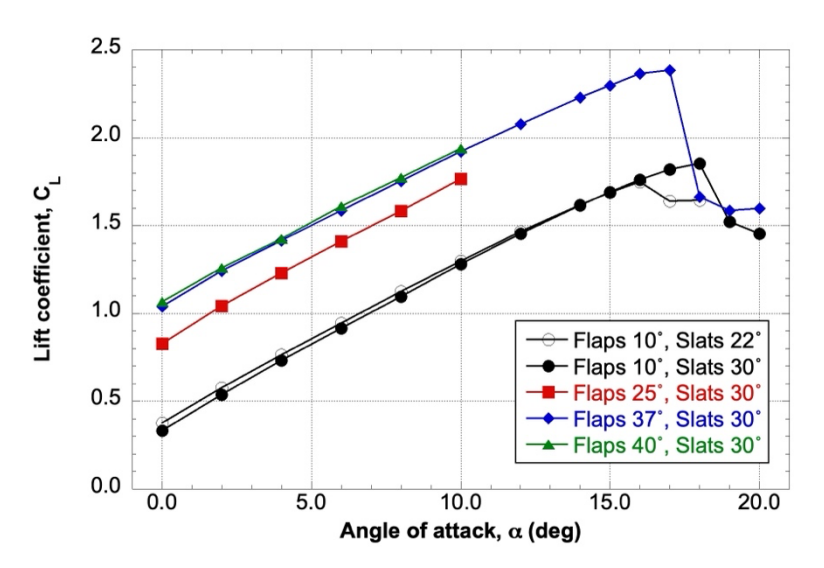


Fig. 1 CFD predicted effect of flap setting on lift for CRM-HL at Re =  $3.26 \times 10^6$ ,  $M_{\infty} = 0.20$ .

In Fig. 2, the CFD predicted effect of flap setting on the lift-to-drag ratio for the CRM-HL without empennage is depicted. Hence, for airplane takeoff and landing performance analysis, a separate prediction of the drag increments of the vertical tail and horizontal tail is required. The results show the impact of slat angle on L/D with the smaller slat angle improving (L/D)<sub>max</sub> from 15.80 to 16.92. In this study, the flaps 10°, slats 22° configuration is used for the takeoff performance analysis.

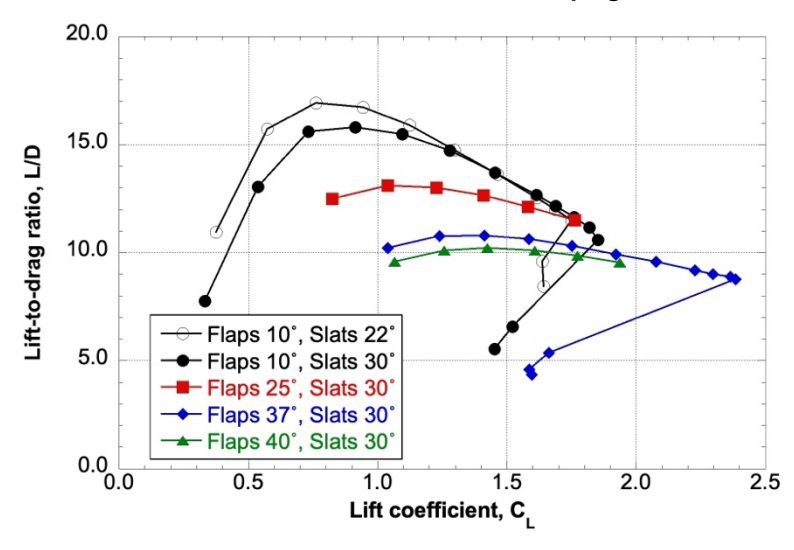


Fig. 2 CFD predicted effect of flap setting on L/D for CRM-HL at Re =  $3.26 \times 10^6$ ,  $M_{\infty} = 0.20$ .

In Fig. 3, the present L/D results for the Flap 37 configuration are compared with the results of Lacy & Sclafani [30] showing good agreement for the relevant range of lift coefficients on approach for landing. The good agreement between these CFD results at very different Reynolds numbers indicates a lack of Reynolds number effect, consistent with the results presented in Ref. [31].

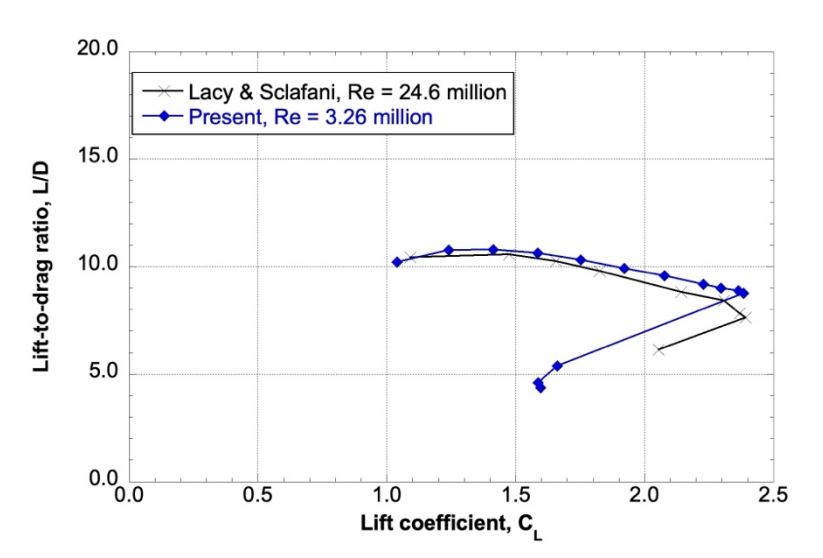


Fig. 3 Comparison CFD predicted L/D for CRM-HL (flaps 37°, slats 30°) and results by Lacy & Sclafani [30] at M<sub>∞</sub> = 0.20.

Analysis of the results of Fig. 2 or Fig. 3 for the airplane in the Flap 37 landing configuration plus accounting for the additional drag generated by the empennage (empennage geometry from Vassberg et al. [35] for the horizontal tail and Atinault & Hue [36] for the vertical tail and the empennage drag contribution determined using the method by Torenbeek [37]) results in the following drag polar (based on least squares fitting of the CFD results for  $\alpha = 0^{\circ}-10^{\circ}$ ):

$$C_D = 0.0885 + 0.0515(C_L - 0.467)^2$$
.

Wind tunnel results presented by Lin et al. [38] indicate a maximum lift coefficient  $C_{L_{max}}$  = 2.46 for the CRM-HL at Flap 37. The above CFD results at the identical Reynolds number and Mach number indicate a slightly lower  $C_{L_{max}}$  = 2.38. Based on the experimental  $C_{L_{max}}$  = 2.46, at the reference landing speed  $V_{REF}$  = 1.23 $V_{SR}$ , where  $V_{SR}$  is the reference (1-g) stall speed,  $C_{L} = C_{L_{max}}/1.23^2 = 1.63$ , resulting in  $C_{D}$  = 0.1576 and  $C_{L}/C_{D}$  = 10.34.

The identical analysis for the airplane in the Flap 10 takeoff configuration (Fig. 2) including the empennage drag, results in the following drag polar (based on least squares fitting of the CFD results for  $\alpha = 2^{\circ}-12^{\circ}$ ):

$$C_D = 0.0344 + 0.0503(C_L - 0.229)^2$$
.

No wind tunnel results are available for the CRM-HL in the Flap 10 takeoff setting with the above CFD results predicting  $C_{L_{max}}$ = 1.75. Based on this prediction, at the minimum takeoff safety speed  $V_2$  = 1.13 $V_{SR}$ ,  $C_L = C_{L_{max}}/1.13^2$  = 1.37, resulting in  $C_D$  = 0.0999 and  $C_L/C_D$  = 13.72.

### 4.1 Auxiliary Power Unit

In this study, the Auxiliary Power Unit (APU) is used as the source of AFC air. An important function of an APU is to provide high-pressure air to the main engine-mounted air turbine starter with air supplied at several times ambient pressure, with the APU sized to enable hot-day main-engine starting. This type of APU is referred to as a pneumatic APU and is especially critical to airplane ETOPS operation. Stohlgren [39] presents detailed performance information on the 331-200 series APU used on the Boeing 757, Boeing 767, and Airbus 310. At standard sea level conditions this APU is capable of a bleed air flow rate of 4.3 lb/s at a pressure of 50 psi. The more capable 331-500 APU installed on the Boeing 777 (and mentioned by Hartwich et al. [16]) is described by Woodhause [40] but little performance information is provided. However, in Ref. [41], it is reported to generate a maximum bleed air flow rate of approximately 8 lb/s.

### 4.2 Conceptual Layout of Microjet Air Supply System

In Fig. 4, the conceptual layout of the AFC air-supply system is depicted including potentially one or more ram air inlets, engine fan bleed, and APU bleed. Note that another option for ram air intakes may well be to locate inlets in the leading edge of each flap and route air into the flap plenum. This is feasible because the flap's attachment-line location and its surface pressure distribution are not significantly affected by airplane angle of attack. The flap deflection angle does change the flap's surface pressure distribution but the attachment-line location on the flap tends to be largely unaffected [42]. The air supply system architectures considered are relatively simple not requiring air storage tanks or additional air compressors.

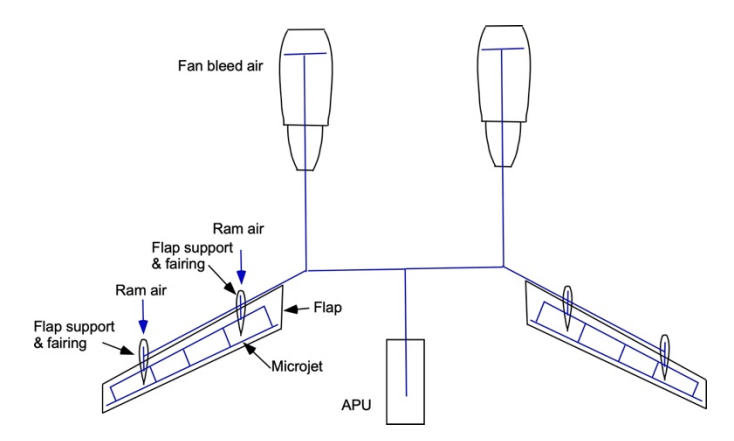


Fig. 4 Conceptual layout of AFC supply system including air from APU and ram air.

### 4.3 Effect of Microjet AFC on CRM-HL Aerodynamic Characteristics

The effects of microjets on the aerodynamic characteristics of the CRM-HL have been studied previously [31, 32]. In these CFD studies, the microjet is modeled using a transpiration boundary condition near the flap trailing edge with much of the focus on the wing-body version in the Flap 37 landing configuration with the slat and flaps deployed at 30° and 37°, respectively. In Fig. 5, the effect of the microjet on the inboard flap at  $\alpha=8.0^\circ$ , Re = 3.26 million, and  $M_\infty=0.20$  is depicted for a range of microjet momentum coefficients. The impact of the inboard flap microjet on the CRM lift curve and drag polar are depicted in Fig. 6 and Fig. 7. The negative impact on drag is the result of the change in spanwise load distribution and hence increase in induced drag caused by the actuation of microjets on the inboard flaps only [32]. This demonstrates that in 3D the impact of any AFC-based lift control on induced drag must be considered from the onset of the development process of any airplane adopting this technology.

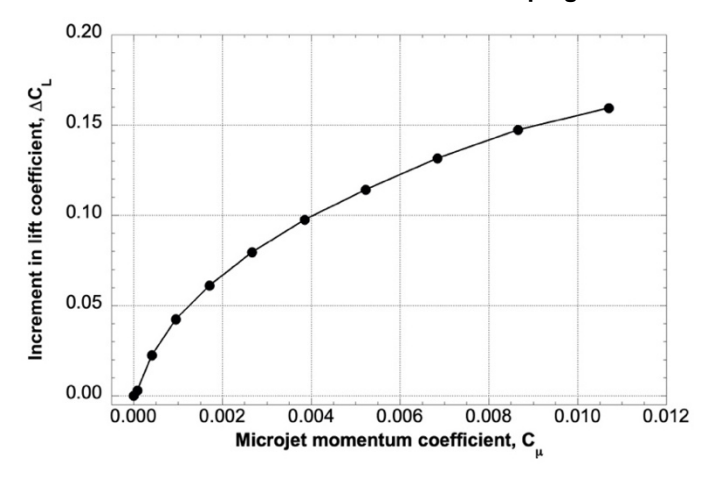


Fig. 5 CFD predicted increment in lift coefficient due to microjet for CRM-HL in Flap 37 configuration at  $\alpha = 8.0^{\circ}$ , Re = 3.26  $\times$  10<sup>6</sup>,  $M_{\odot}$  = 0.20. Microjet implemented on inboard flap only on pressure-side at 95% of flap chord.

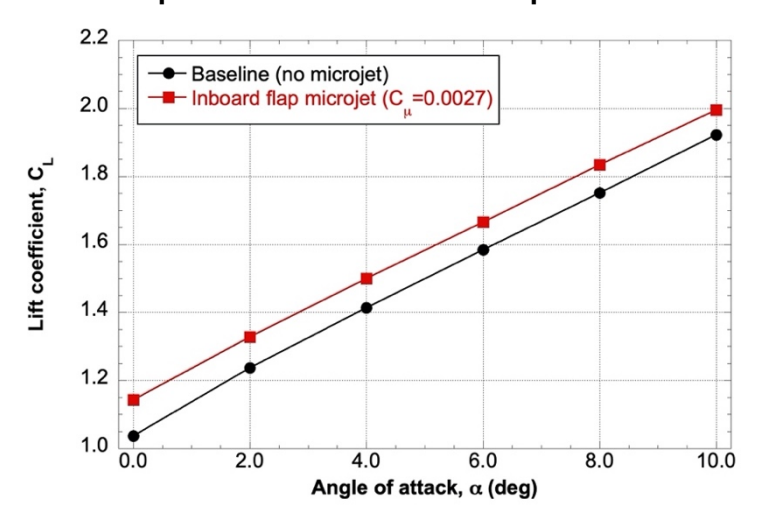


Fig. 6 CFD-based lift curves for CRM-HL in Flap 37 configuration at Re =  $3.26 \times 10^6$ ,  $M_{\infty}$  = 0.20. Microjet implemented on inboard flap only on pressure-side at 95% of flap chord.

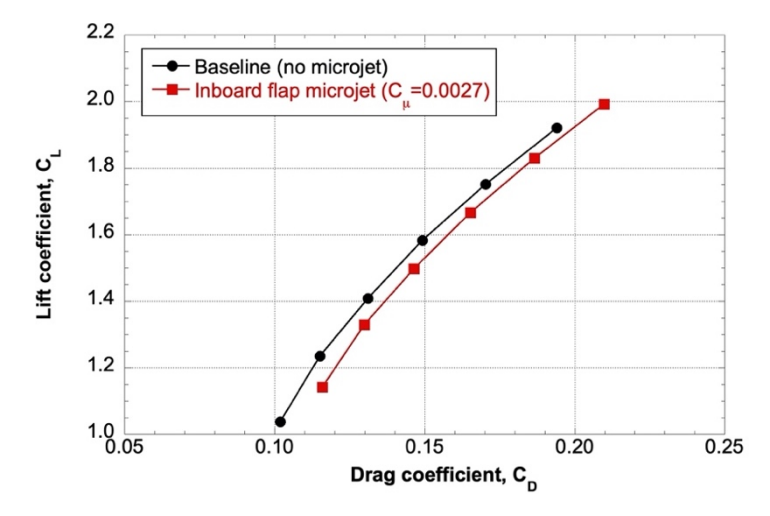


Fig. 7 CFD-based drag polars for CRM-HL in Flap 37 configuration at Re =  $3.26 \times 10^6$ ,  $M_{\odot}$  = 0.20. Microjet implemented on inboard flap only on pressure-side at 95% of flap chord.

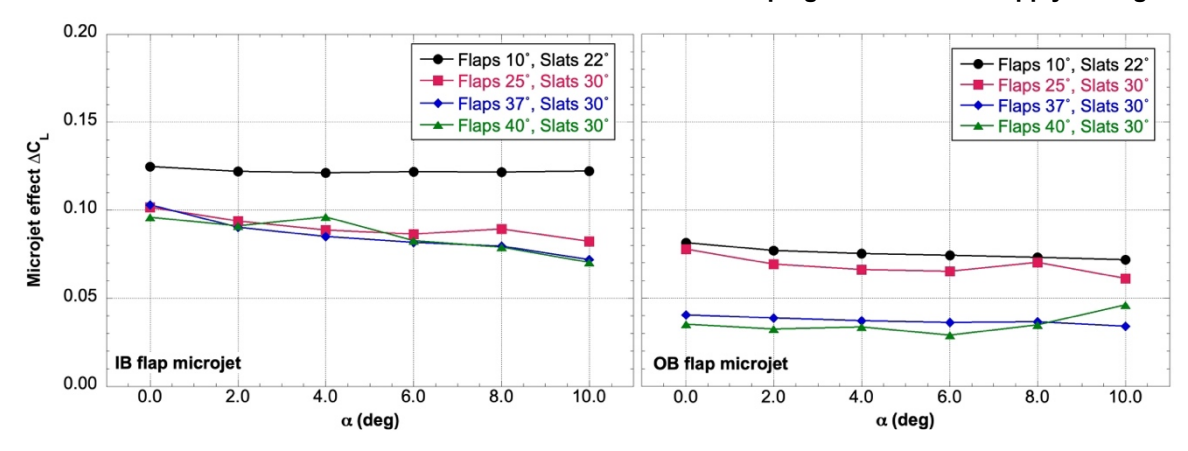


Fig. 8 CFD predicted increment in lift coefficient due to microjet for CRM-HL at Re = 3.26  $\times$  106,  $M_{\infty}$  = 0.20. Microjet at 95% of flap chord activated on inboard flap at  $C_q$  = 0.0013,  $C_{\mu}$  = 0.0027 (left) and outboard flap at  $C_q$  = 0.0010,  $C_{\mu}$  = 0.0020 (right).

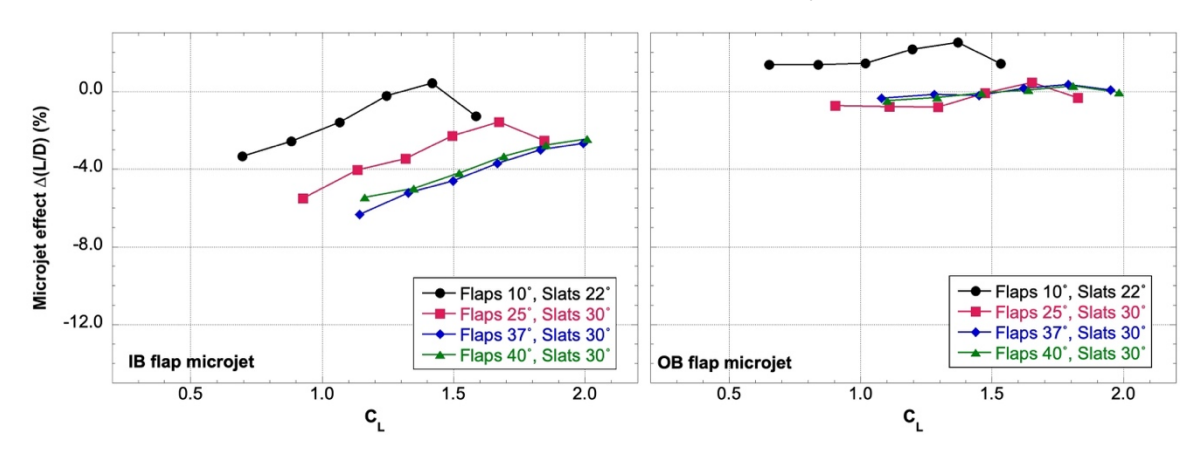


Fig. 9 CFD predicted increment in L/D due to microjet for CRM-HL at Re =  $3.26 \times 10^6$ ,  $M_{\infty}$  = 0.20. Microjet at 95% of flap chord activated on inboard flap  $C_q$  = 0.0013,  $C_{\mu}$  = 0.0027 (left) and outboard flap at  $C_q$  = 0.0010,  $C_{\mu}$  = 0.0020 (right).

In this paper, the focus is on the impact of microjets on CRM lift and lift-to-drag ratio (L/D) during takeoff. Given the uncertainty related to CFD-based  $C_{Lmax}$  predictions [43] only conditions in the linear lift regime are considered. In Fig. 8 and Fig. 9, the changes in lift as function of angle of attack and L/D as a function of lift coefficient are summarized for microjets on the inboard flaps and the outboard flaps and a range of flap settings. For the microjet configuration studied here, the microjet slot in the outboard flaps is tapered resulting in a slightly lower mass flow coefficient for constant  $V_{jet}/V_{\infty} = 1.0$ , resulting in  $C_q = 0.0010$  for outboard flap compared to  $C_q = 0.0013$  for inboard flap microjets. The major conclusions derived from Fig. 8 and Fig. 9:

- For the range of angles of attack considered, the microjet-based lift increment is largely independent of angle of attack for all flap settings.
- Microjet activation on the inboard flaps creates a larger lift increment than activation on the outboard flaps.
- After accounting for the different mass flow coefficients, the differences in lift increment between inboard and outboard flap activation are smaller. For Flap 10,  $\Delta C_L/C_q \approx 94$  for inboard flap microjets and  $\Delta C_L/C_q \approx 74$  for outboard flap microjets.
- When considering the impact of microjet activation on airplane L/D for  $1.0 \le C_L \le 2.0$ , activation of microjets on the inboard flaps causes L/D to decrease whereas outboard flap microjets increase L/D for Flap 10 and have a mostly negligible effect on L/D for the higher flap settings.

Note, the results for Fig. 8 and Fig. 9 are generated for a wind tunnel Reynolds number Re = 3.26 million, well below a typical full-scale Reynolds number on takeoff or landing. Based on the comparisons between wind-tunnel and full-scale flight Reynolds number results presented in Ref. [31], the effect of Reynolds number on the impact of the microjets on lift and drag is small, and hence the Re = 3.26 million results provide acceptable accuracy for this scoping study.

## 5. Methodology

The analysis of the air supply systems is based on the 1D compressible flow with friction equations with two architectures considered in this paper: (1) APU bleed air plus ram air, and (2) fan bleed air plus ram air. To allow for a mixture of two air supplies with very different pressures, a supersonic ejector model is introduced to analyze the combination of high-pressure APU bleed and low-pressure ram air. Ejectors are commonly used to efficiently mix two flows of very different pressures and to control flow temperatures as, e.g., on the Lockheed 1011 where air extracted from the high-pressure engine compressor is mixed with air from the intermediate pressure engine compressor to limit bleed air temperatures [44]. The pressure of the fan bleed air is too low to reach critical conditions and, hence, a subsonic nozzle model is used to analyze the combination of medium-pressure fan bleed air and low-pressure ram air. In Fig. 10 the flow path diagrams are shown for these two air supply architectures.

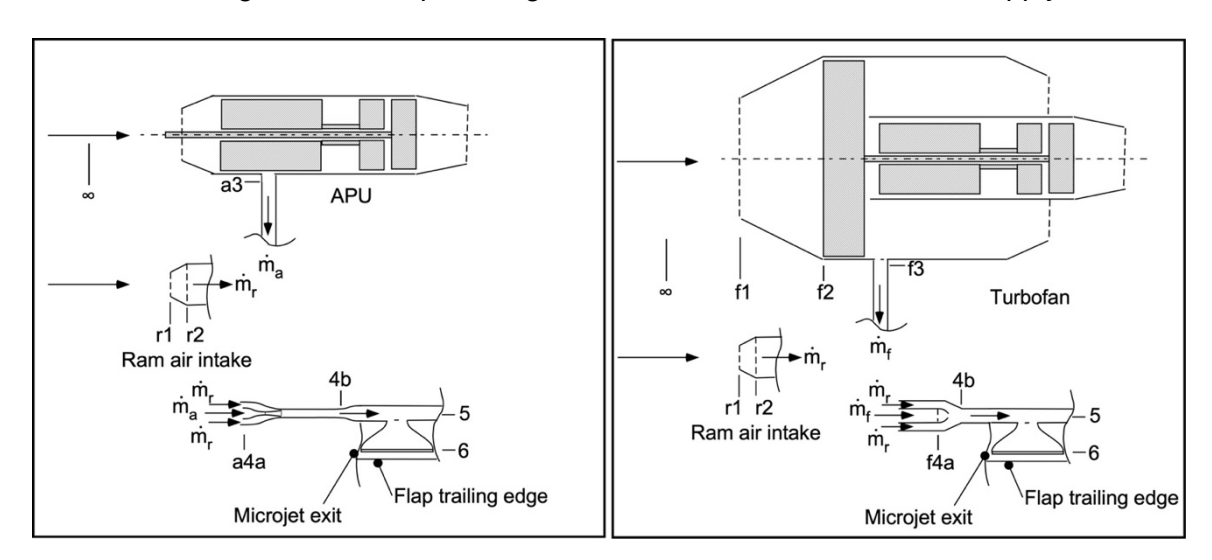


Fig. 10 Sketch of AFC air supply paths and stations for APU bleed plus ram air (left) and fan bleed plus ram air (right). Various system components not to scale.

In Fig. 10, the AFC flow path stations are shown from freestream ( $\infty$ ) to the microjet exit (station 6) with air from an APU,  $\dot{m}_a$ , or engine fan bleed,  $\dot{m}_f$ , used to entrain ram air,  $\dot{m}_r$ . Because of the very different pressures of the bleed air and ram air, care must be taken in mixing them. The pressure of the APU air is sufficiently high to consider a converging-diverging supersonic ejector (shown in Fig. 10 just downstream of station a4a) to entrain the low-pressure ram air and thereby increase the mass flow rate available for the microjet. The 1D ejector model follows the works by Huang et al. [45] and Chen et al. [46] and is presented in Ref. [12]. Application of the 1D ejector model allows determination of the mixed mass flow  $\dot{m}_j$  of the microjet (conservation of mass), velocity  $v_5$  (momentum equation), and temperature  $T_5$  (energy equation). A nozzle with an isentropic efficiency  $\eta_j$  then connects this conduit to the microjet exit to achieve the microjet pressure  $p_6$  and its velocity  $v_6 = V_{jet}$ . The pressure of the fan bleed is too low to achieve critical flow conditions and, hence, a simple converging nozzle (shown in Fig. 10 between stations f4a and 4b) is used for the fan bleed to mix with and power the ram air. A detailed description of the methodologies is presented in Ref. [12].

## 6. Results & Discussion

In Ref. [12], the authors studied various air supply architectures with the focus on the impact of a microjet-based AFC system on the lift coefficient at the angle of attack limited by the tail clearance angle on landing. Here, we consider the air supply systems discussed in Section 5 for a microjet-based AFC system on the CRM-HL flaps at standard sea level conditions at  $V_{\infty} = 175$  knots ( $M_{\infty} = 0.265$ ) on a second segment climb gradient limited takeoff.

#### 6.1 APU Bleed Plus Ram Air

As stated earlier, APUs can provide a limited supply of air at relatively high pressure. By supplementing this limited air supply by entraining ram air, effective microjet-based flow control may be achievable. An additional advantage of ram air entrainment is that it lowers the temperature of the AFC air without the addition of a heat exchanger.

The APU is assumed to be capable of supplying 8 lb/s of bleed air at PR = 4.0. This bleed air then feeds eight ejectors with a constant high pressure air input of 1.0 lb/s each, pressure  $p_{t_{a3}}$ = 8,710 lb/ft² and temperature  $T_{t_{a3}}$  = 826 °R during takeoff (8,559 lb/ft² and 823 °R during landing). The ejector nozzle throat diameter is 1.08 in. and its nozzle exit diameter is 1.53 in. In Fig. 11 the calculated ejector compression ratio (ratio of the total pressure at the ejector exit and the total pressure at the exit of the ram air inlet) and air entrainment ratio (ratio of the ram air flow and high pressure APU air flow) are shown as a function of the ratio of the ejector cross section area and the fixed high-pressure flow nozzle throat area (=  $\frac{\pi}{4}$ 1.08² = 0.92 in²). The latter ratio ranges from 5 to 20 for an ejector diameter from 2.1 in. to 4.1 in. The results of Fig. 11 demonstrate that ram air entrainment increases with increasing ejector cross sectional area. However, with increasing entrainment of this low-pressure air flow, the achievable compression ratio drops.

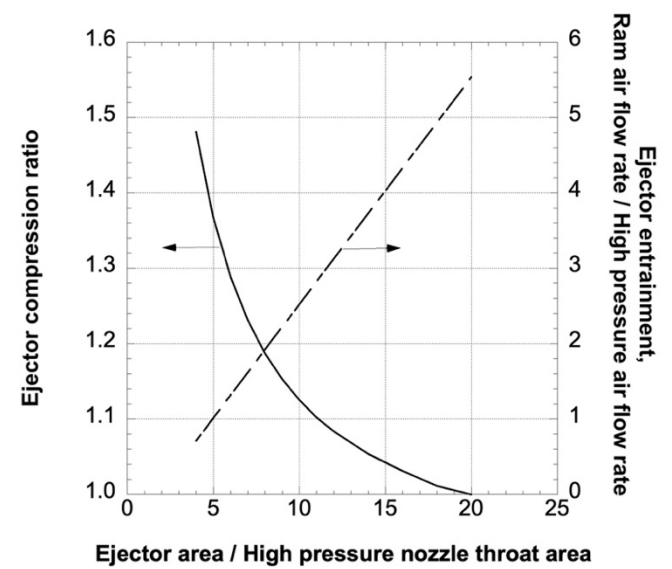


Fig. 11 Predicted ejector performance characteristics for fixed high pressure nozzle throat area (0.92 in<sup>2</sup>), high pressure (APU bleed) air flow rate ( $\dot{w}_a$  = 1.0 lb/s) at takeoff conditions.

For a given APU bleed pressure, the ejector performance depends on the back pressure which is governed by (1) the local surface pressure on the flap at the microjet exit, and (2) the desired microjet velocity ratio  $V_{\rm jet}/V_{\infty}$ . A static pressure coefficient  $C_p = 0.10$  is selected for the pressure at the microjet exit. This is a typical value observed on the pressure side of a flap near the trailing edge as e.g. shown by Yip et al. [47] for the Boeing 737 aft flap. Future study will include a sensitivity analysis to assess the effect of the parameters selected in the study (including  $C_p$  at the microjet exit) on the performance of architecture. The maximum microjet Mach number was kept below 0.8 with higher microjet velocities resulting in higher jet-related noise levels. With increasing back pressure (increasing ejector pressure ratio), the amount of ram air the ejector can entrain reduces. In Table 1 the resulting ram and total airflow rates are presented for a wide range of microjet velocities.

Table 1 Amount of ram air flow  $\dot{w}_r$  (lb/s) entrained as a function of microjet velocity ratio at a microjet surface pressure coefficient of 0.1 and takeoff conditions.

Microjet	Ejector	APU air	Ram air	Microjet	Microjet	Microjet
velocity	diameter,	weight	weight	weight	Mach	total
ratio,	in.	flow	flow rate,	flow rate,	number	pressure
$V_{jet}/V_{\infty}$		rate, wa	w॑ <sub>r</sub> (lb/s)	ẅ <sub>j</sub> (lb/s)		ratio,
		(lb/s)		,		$p_{t_6}/p_{t_\infty}$
3.2	2.22	8 × 1.0	8 × 0.77	14.20	0.77	1.42
3.0	2.34	8 × 1.0	8 × 0.92	15.36	0.73	1.36
2.5	2.67	8 × 1.0	8 × 1.34	18.72	0.61	1.23
2.0	3.04	8 × 1.0	8 × 1.89	23.12	0.49	1.13
1.5	3.45	8 × 1.0	8 × 2.57	28.56	0.37	1.05
1.0	3.85	8 × 1.0	$8 \times 3.33$	34.64	0.25	1.00

Next, the impact of these architectures on the mission performance of the CRM is considered. As pointed out by Brooks et al. [48], the CRM resembles the Boeing 777-200ER in terms of size and performance. Based on the performance characteristics of this airplane, the CRM mission considered involves a takeoff weight (MTOW) of 656,098 lb carrying a payload of 74,800 lb over a distance of 7,725 nm at a cruise Mach number of 0.84 and an initial cruise altitude of 36,000 ft. The baseline airplane (no AFC) has an operating empty weight (OEW) of 304,511 lb and will require 243,592 lb of fuel plus 33,075 lb of reserve fuel.

The scenario considered involves the use of APU bleed air and ram air to supply the microjets to improve the airplane's performance characteristics during takeoff. On takeoff, L/D is critical on account of the second segment climb gradient requirement of 0.024 for twin-engine civil transport airplanes with one engine inoperative (OEI). For the baseline CRM (Flap 10, no AFC) on a second-segment gradient limited takeoff, L/D =13.03 (reduced from L/D listed in Section 4 to account for asymmetric thrust trim effects). A 1.0% increase in takeoff L/D is equivalent to a 4,986 lb increase in maximum takeoff weight resulting in, after accounting for weight related extra mission fuel, a 3,135 lb increase in payload for the mission considered in this scoping study. Note this compares well with the impact of L/D noted by Meredith [49] who indicates a 2,800 lb increase in payload for a 1% increase in takeoff L/D for a CRM size twin-engine transport on a second segment climb gradient limited takeoff, with the discrepancy likely related to a different airplane mission considered in this study. Given the L/D results of Fig. 9 and the indicated L/D penalty linked to inboard flap microjets, microjets on the outboard flaps only are selected with a notable increase in L/D observed for Flap 10. Based on Table 1, the maximum of the product of weight flow rate and microjet velocity,  $\dot{w}_j V_{jet} = (\dot{w}_a + \dot{w}_r) V_{jet}$ , and, hence, maximum momentum coefficient is achieved for  $V_{jet}/V_{\infty} = 2.5$ . However, to reduce the intake of ram air and the related drag penalty, the near-optimum  $V_{jet}/V_{\infty}=3.2$  is selected, resulting in a  $C_{\mu}=0.0010$  for a lift curve shift,  $\Delta C_L = +0.050$  and an  $\Delta \left(\frac{L}{D}\right) = 1.25$  %. The latter improvement is equivalent to a decrease in drag coefficient of 12.5 counts at constant lift coefficient. However, the corresponding ram air intake of 6.2 lb/s causes a drag penalty of 1.3 drag counts on takeoff [12]. The combination of these two effects results in an improvement in takeoff L/D of 1.12 %. On a second segment climb gradient limited takeoff, this is equivalent to a 5,583 lb increase in allowable takeoff weight and, after accounting for the increase in OEW (estimated AFC system weight) of 304 lb and the change in fuel burn on account of the higher takeoff weight, a 3,206 lb increase in payload results for the mission considered in this initial scoping study.

### 6.2 Fan Bleed Plus Ram Air

Next, the combination of fan bleed air and ram air is considered. To facilitate comparison, the target microjet momentum coefficient is unchanged, C<sub>u</sub> = 0.0010. Fan bleed ratios for high bypass ratio engines are modest (here FPR = 1.58 on takeoff) limiting the ram air to bleed air entrainment ratios that can be achieved. Also, on account of the lower pressures, a non-critical converging nozzle is used to mix the two air flows. In Table 2, the ram air flow rates as a function of fan bleed air flow rates are calculated for a range of the microjet velocity ratios and the static pressure coefficient of 0.1. Based on the results presented in Table 2, the maximum of the product of weight flow rate and microjet velocity,  $\dot{w}_i V_{jet} = (\dot{w}_f + \dot{w}_r) V_{jet}$ , and, hence, maximum momentum coefficient is achieved for  $V_{jet}/V_{\infty} = 1.0$ . At  $\dot{w}_j = 2 \times 6.0$  lb/s and  $V_{jet}/V_{\infty} = 1.0$ , the computations indicate  $\dot{w}_r = 2 \times 16.68$  lb/s for a matching momentum coefficient  $C_{\mu}$  = 0.0010 and, as indicated in Section 6.1, a decrease in drag coefficient of 12.5 counts at constant lift coefficient. The ram air intake causes a drag penalty of 7.1 drag counts on takeoff [12]. In addition, the 6.0 lb/s of fan bleed air per engine on takeoff out of a total air intake of 2,977 lb/s per engine [50] is predicted to decrease the thrust by 0.20% or an equivalent drag increase of 0.20%. The combination of these three effects results in an improvement in takeoff L/D of 0.34%. On a second segment climb gradient limited takeoff, this is equivalent to a 1,695 lb increase in allowable takeoff weight. The impact of the AFC system on airplane OEW depends on how much of the airplane's existing bleed air infrastructure can be shared for AFC air supply. If fan bleed is solely used for AFC, then the ducting connecting the engine to the flap is significant adding notable weight. Applying 0.10 in. thick, 6.0 in. diameter, 321 CRES (corrosion-resistant steel) ducting with a length of 20 ft per side, the additional weight is  $2 \times 131$  lb = 262 lb. The required system space and possible weight penalties are key reasons why AFC should be considered early in the design of an airplane. However, assuming

the identical OEW increase as used in Section 6.1 (304 lb) and the change in fuel burn on account of the higher takeoff weight, a 762 lb increase in payload results for the mission considered in this initial scoping study.

Table 2 Amount of ram air flow  $\dot{w}_r$  (lb/s) entrained as a function of fan bleed air flow rate  $\dot{w}_f$  (lb/s) and microjet velocity ratio  $V_{jet}/V_{\infty}$  at a microjet surface pressure coefficient of 0.1 and takeoff conditions. Conduit diameter d = 6 in.

$\begin{array}{c} \text{Microjet velocity ratio} \\ V_{\text{jet}}/V_{\infty} \rightarrow \\ \text{Fan bleed } \dot{w}_f \downarrow \end{array}$	1.0	1.5	2.0
2 × 5.0	2 × 14.14	2 × 5.43	2 × 2.39
2 × 6.0	2 × 16.68	2 × 6.35	2 × 2.76
2 × 7.0	2 × 19.07	$2 \times 7.20$	$2 \times 3.07$
2 × 8.0	2 × 21.30	$2 \times 7.95$	$2 \times 3.31$
2 × 9.0	$2 \times 23.37$	2 × 8.62	$2 \times 3.50$
2 × 10.0	$2 \times 25.33$	2 × 9.23	$2 \times 3.64$

#### 6.3 Other Takeoff Performance Considerations

As explained by Meredith [49], an increase in lift coefficient for a given angle of attack can have a significant effect on the airplane attitude angle and, hence, landing gear height on approach for landing. However, on takeoff the shift in the lift curve can also have a significant effect on the minimum unstick speed  $(V_{\text{MU}})$  of the CRM. For many FAR 25 regulated airplanes, the minimum takeoff speed and, consequently, takeoff distance, are not governed by the maximum lift coefficient but by  $V_{\text{MU}}$ .  $V_{\text{MU}}$  is determined by rotating the airplane to its maximum angle of attack (which for longer-bodied configurations such as the CRM is dictated by the tail clearance angle) while slowly increasing takeoff speed. The lowest speed at which the airplane lifts off and climbs safely out of ground effect is  $V_{\text{MU}}$ . The impact of  $V_{\text{MU}}$  on takeoff performance is illustrated in Fig. 12. Given the complexity of  $V_{\text{MU}}$  modeling, the impact of the lift curve shift on  $V_{\text{MU}}$  cannot be determined as part of this scoping study, but its impact on mission performance will be considered in future studies.

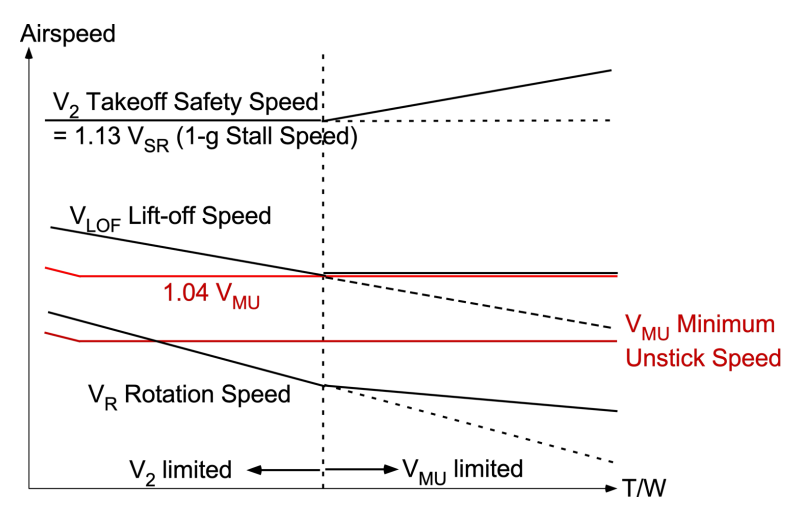


Fig. 12Impact of  $V_{MU}$  on takeoff performance. At lower thrust-to-weight ratios (T/W), takeoff performance is governed by  $V_2$  (i.e.,  $C_{Lmax}$ ). At higher T/W,  $V_{LOF}$  is governed by  $V_{MU}$ . As  $V_R$ ,  $V_{LOF}$  and  $V_2$  increase, takeoff field length is increased. Illustration adapted from Slingerland [51].

### 7. Conclusions and Next Steps

An initial scoping study was conducted on the air supply of a microjet-based active flow control (AFC) system on a long-range, twin-engine, commercial transport airplane. In this study, microjets are considered for installation in the flaps of the twin-engine Common Research Model (CRM-HL) with the main intent to control the lift in the linear regime where the airplane operates during takeoff and landing. As such, the microjets allow for a more granular control of lift in the high-lift flight phases compared to the control provided by a limited number of fixed flap settings (where it should be noted that the intent is to gain more control over lift and its spanwise distribution at constant angle of attack and not to

#### Scoping of an AFC Air Supply Configuration

replace the flaps). The sources of air considered in this initial scoping study are (1) a combination of APU bleed and ram air and (2) a combination of fan bleed and ram air, where the bleed air is used to entrain and power the ram air thereby increasing the mass flow and momentum available for the microjet lift control system. In this study, a simple 1-D flow model was developed and applied to predict the performance of compressible duct flows including viscous losses and the mixing of flows of different pressures.

The amount of bleed air available from an APU is limited. However, by using this high-pressure air to entrain ram air, this AFC architecture to supply microjets on the flaps is predicted to be able to make notable improvements in the performance characteristics of the CRM. The scenario considered in this paper involves microjets on the outboard flaps during takeoff (second segment climb gradient limited) predicted to generate a lift curve shift  $\Delta C_L = +0.050$  and most importantly a  $\Delta \left(\frac{L}{D}\right) = 1.25\%$  equivalent to a decrease in drag coefficient of 12.5 counts. After accounting for the ram air drag penalty, the increase in OEW (estimated AFC system weight), and the change in mission fuel burn, a 3,206 lb (approximately 16 passengers) increase in payload is predicted for the long-range mission with a second segment climb gradient limited takeoff considered in this study.

The second architecture studied involved fan bleed air in combination with ram air. The amount of bleed available from just downstream of the fan is more abundant but the pressure is much lower than available from the APU thereby limiting the ram air to bleed entrainment ratio. For the same microjet momentum coefficient, and after accounting for the ram air drag penalty, the withdrawal of bleed air on engine thrust, the increase in OEW (estimated AFC system weight), and the change in mission fuel burn, a 706 lb (3 - 4 passengers) increase in payload is predicted for the long-range mission with a second segment climb gradient limited takeoff. The significant improvements and differences in predicted mission performance between these two AFC air supply architectures clearly demonstrates the importance of considering an AFC technology such as microjets and its flow benefits early in the design of commercial transport airplanes while in parallel analyzing its impact on the overall airplane system.

Study of the air supply of a microjet-based AFC system on a twin-turbofan, commercial transport airplane for lift control during takeoff and landing underscores:

- The complexities of takeoff and landing performance analysis and optimization for long-bodied, twin-engine, civil transport airplanes
- The sensitivity of airplane drag to the spanwise location of AFC-based lift control and the importance of considering the impact on the spanwise lift distribution and induced drag during the initial design stages
- The relatively low air supply pressures needed for an effective microjet-based lift control system.
- The opportunity to use excess pressure of the air supplied by the APU or engines to, through the application of ejectors or nozzles, entrain ram air and thereby enhance the effectiveness of the AFC-based lift control system

#### Future work should focus on:

- Conducting a sensitivity analysis to assess the effect of the parameters selected in this study on the performance of the AFC air supply architectures
- Detailed weight and performance analysis of the various AFC air supply architectures including detailed CFD analysis of the ejector model used to entrain ram air
- Including engine core bleed in the AFC air supply architectures studied
- Considering the effect of reduced engine thrust conditions on engine bleed air pressure ratios during approach for landing conditions
- Evaluating the impact of microjet actuation on C<sub>Lmax</sub> for the airplane in the landing configuration
  (as indicated by Meredith [49] for a CRM-size airplane, an increase in C<sub>Lmax</sub> of 1.5% may
  produce a 6,600 lb increase in mission payload for a fixed approach speed)
- Studying in more detail the impact of a microjet-induced lift shift on V<sub>MU</sub> and, for a fixed takeoff distance, the mission performance of the airplane
- Extension to different missions including takeoff from a high-density-altitude airport such as a Denver flight to Honolulu
- Extension to smaller commercial airplane configurations

Lastly, the full integration of AFC technology into civil transport airplanes still faces challenges due to its complexity, cost, power & space requirements, weight penalties, and certification hurdles [52]. To overcome these challenges and take full advantage of the performance and control opportunities provided by AFC, application of this technology must be considered right from the initial stages of airplane design by considering not only the flow benefits but also the impacts on the total airplane system as well as possible synergistic configuration opportunities.

## 8. Contact Author Email Address

Mail to: cpvandam@ucdavis.edu

## 9. Copyright Statement

The authors confirm that they, and/or their company or organization, hold copyright on all of the original material included in this paper. The authors also confirm that they have obtained permission, from the copyright holder of any third party material included in this paper, to publish it as part of their paper. The authors confirm that they give permission, or have obtained permission from the copyright holder of this paper, for the publication and distribution of this paper as part of the ICAS proceedings or as individual off-prints from the proceedings.

## 10. Acknowledgments

The research reported in this paper is funded by NASA's Advanced Air Transport Technology project. The work by the University of California–Davis is funded under agreements 80NSSC21K0473, 80NSSC22K0985, and 80NSSC24K0122.

#### References

- [1] Flaig, A., and Hilbig, R., "High-Lift Design for Large Civil Aircraft," *High-Lift System Aerodynamics*, AGARD CP-515, 1993, pp. 31–1-31–12.
- [2] Nield, B. N., "An Overview of the Boeing 777 High Lift Aerodynamic Design," *Aeronautical Journal*, Vol. 99, Nov. 1995, pp. 361–371. https://doi.org/10.1017/S0001924000028670
- [3] Rudolph, P.K.C., "High-Lift Systems on Commercial Airliners," NASA CR-4746, Sep. 1996. https://ntrs.nasa.gov/api/citations/19960052267/downloads/19960052267.pdf
- [4] Reckzeh, D., "Aerodynamic Design of the High-Lift Wing for a Megaliner Aircraft," *Aerospace Science & Technology*, Vol. 7, March 2003, pp. 107–119. https://doi.org/10.1016/S1270-9638(02)00002-0
- [5] De Resende, O. C., "The Evolution of the Aerodynamic Design Tools and Transport Aircraft Wings at Embraer," *Journal of the Brazilian Society of Mechanical Sciences and Engineering*, Vol. 26, No. 4, 2004, pp. 379–390. https://doi.org/10.1590/s1678-58782004000400004
- [6] Kafyeke, F., Pépin, F., and Kho, C., "Development of High-Lift Systems for the Bombardier CRJ-700," 23rd International Congress of Aeronautical Sciences, ICAS Paper 2002-3.10.1, Sep. 2002.
- [7] Van Dam, C.P., "The Aerodynamic Design of Multi-Element High-Lift Systems for Transport Airplanes," Progress in Aerospace Sciences, Vol. 38, 2002, pp. 101-144. https://doi.org/10.1016/S0376-0421(02)00002-7
- [8] Hosseini, S.S., "Computational Investigations of Surface-Normal Pneumatic Active Load Control for Lift Enhancement and Separation Mitigation in High-Lift Systems," PhD Dissertation, University of California, Davis, Jun. 2020.
- [9] Hosseini, S.S., van Dam, C.P., and Pandya, S.A., "Aerodynamic Load Control for Multi-Element Airfoils Using Surface-Normal Trailing-Edge Blowing," *Journal of Aircraft*, Vol. 56, No. 4, 2019, pp. 1668-1676. https://doi.org/10.2514/1.C035248
- [10] Hosseini, S.S., Cooperman, A.C., van Dam, C.P., and Pandya, S.A., "Microjet Configuration Sensitivities for Active Flow Control on Multi-Element High-Lift Systems," *Journal of Aircraft*, Vol. 58, No. 4, 2021, pp. 743–761. https://doi.org/10.2514/1.C035986
- [11] Van Dam, C.P., Mothukuri, S.B., Hosseini, S.S., White, E.B., Brown, L.M., Kutz, D.M., and Justiniano, E., "Wind Tunnel Experiment of Microjet-Based Flow Control on a Two-Dimensional Wing with Flap," *Journal of Aircraft*, Vol. 60, No. 2, 2022, pp. 577–580. https://doi.org/10.2514/1.C036864
- [12] Van Dam, C.P., Hosseini, S.S., and Pandya, S.A., "Scoping of an Air Supply System for Active Flow Control on a Commercial Transport Airplane," AIAA Paper 2024-1934, Jan. 2024. https://doi.org/10.2514/6.2024-1934
- [13] Englar, R.J., Hemmerly, R.A., Moore, W.H., Seredinsky, V., Valckeraere, W., and Jackson, J.A., "Design of the Circulation Control Wing STOL Demonstrator Aircraft," *Journal of Aircraft*, Vol. 18, No. 1, 1981, pp. 51-58. https://doi.org/10.2514/3.57463

- [14] Englar, R.J., Smith, M.J., Kelley, S.M., and Rover III, R.C., "Application of Circulation Control to Advanced Subsonic Aircraft, Part II: Transport Application," *Journal of Aircraft*, Vol. 31, No. 5, 1994, pp. 1169-1177. https://doi.org/10.2514/3.46627
- [15] Werner-Spatz, C., Heinze, W., Horst, P., and Radespiel, R., "Multidisciplinary Conceptual Design for Aircraft with Circulation Control High-Lift Systems," *CEAS Aeronautical Journal*, Vol. 3, No. 2-4, 2012, pp. 145-164. https://doi.org/10.1007/s13272-012-0049-5
- [16] Hartwich, P.M., Dickey, E.D., Sclafani, A.J., Camacho, P., Gonzales, A.B., Lawson, E.L., Mairs, R.Y., and Shmilovich, A., "AFC-Enabled Simplified High-Lift System Integration Study," NASA/CR-2014-218521, Sep. 2014. https://ntrs.nasa.gov/api/citations/20140012783/downloads/20140012783.pdf
- [17] Hartwich, P.M., Shmilovich, A., Lacy, D.S., Dickey, E.D., Sclafani, A.J., Sundaram, P., and Yadlin, Y., "Refined AFC-Enabled High-Lift System Integration Study," NASA/CR-2016-219170, Mar. 2016. https://ntrs.nasa.gov/api/citations/20160006410/downloads/20160006410.pdf
- [18] Mooney, H.P., Brandt, J.B., Lacy, D.S., and Whalen, E.A., "AFC-Enabled Vertical Tail System Integration Study," NASA/CR-2014-218168, Mar. 2014. https://ntrs.nasa.gov/api/citations/20140003900/downloads/20140003900.pdf
- [19] Alexander, M.G., Harris, F.K., Spoor, M.A., Boyland, S.R., Farrell, T.E., and Raines, D.M., "Active Flow Control (AFC) and Insect Accretion and Mitigation (IAM) System Design and Integration on the Boeing 757 ecoDemonstrator," AIAA Paper 2016-3746, Jun. 2016. https://doi.org/10.2514/6.2016-3746
- [20] Whalen, E.A., Shmilovich, A., Spoor, M., Tran, J., Vijgen, P., Lin, J.C., and Andino, M., "Flight Test of an Active Flow Control Enhanced Vertical Tail," *AIAA Journal*, Vol. 56, No. 9, Sep. 2018, pp. 3393-3398. https://doi.org/10.2514/1.J056959
- [21] Bertels, F.G., van Dijk, R., Elmendorp, R., and Vos, R., "Impact of Pulsed Jet Actuators on Aircraft Mass and Fuel Consumption," *CEAS Aeronautical Journal*, Vol. 7, No. 4, 2016. https://doi.org/10.1007/s13272-016-0201-8
- [22] Woszidlo, R., Shmilovich, A., and Vijgen, P., "Low-Speed Performance Enhancement Using Localized Active Flow Control: Program Overview and Summary (1/4)," NASA Contractor Report, Apr. 2022. https://ntrs.nasa.gov/api/citations/20220006728/downloads/1-Program%20Overview-Unlimited%20Rights.pdf
- [23] Shmilovich, A., Vijgen, P., and Woszidlo, R., "Low-Speed Performance Enhancement Using Localized Active Flow Control: Localized Active Flow Control Simulations on a Reference Aircraft (2/4)," NASA Contractor Report, Apr. 2022. https://ntrs.nasa.gov/api/citations/20220006731/downloads/2-CFD%20on%20Reference%20Aircraft
  - https://ntrs.nasa.gov/api/citations/20220006731/downloads/2-CFD%20on%20Reference%20Aircraft-Unlimited%20Rights.pdf
- [24] Vijgen, P., Ziebardt, A., Shmilovich, A., and Woszidlo, R., "Low-Speed Performance Enhancement Using Localized Active Flow Control: Integration Study of Localized Active Flow Control on a Reference Aircraft (3/4)," NASA Contractor Report, Apr. 2022. https://ntrs.nasa.gov/api/citations/20220006733/downloads/3-
  - Integration%20Study%20on%20Refence%20Aircraft-UnLimited%20Rights.pdf
- [25] Shmilovich, A., Stauffer, M., Woszidlo, R., and Vijgen, P., "Low-Speed Performance Enhancement Using Localized Active Flow Control: Simulations, Scaling, and Design of Localized Active Flow Control on the Common Research Model (4/4)," NASA Contractor Report, Apr. 2022. https://ntrs.nasa.gov/api/citations/20220006736/downloads/4-CRM%20Summary-Unlimited%20Rights.pdf
- [26] Cai, Y., Gao, Z., Chakraborty, I., Briceno, S., and Mavris, D.N., "System-Level Assessment of Active Flow Control for Commercial Aircraft High-Lift Devices," *Journal of Aircraft*, Vol. 55, No.3, 2018, pp. 1200-1216. https://doi.org/10.2514/1.C034401
- [27] Shmilovich, A., and Whalen, E., "Strategies for Practical Implementations of Low-Input Thermal Flow Control," AIAA Paper 2019-0886, Jan. 2019. https://doi.org/10.2514/6.2019-0886
- [28] Daggett, D.L., Brown, S.T., and Kawai, R.T., "Ultra-Efficient Engine Diameter Study," NASA/CR-2003-212309, May 2003. https://ntrs.nasa.gov/api/citations/20030061085/downloads/20030061085.pdf
- [29] Vassberg, J., DeHaan, M., Rivers, M., and Wahls, R., "Development of a Common Research Model for Applied CFD Validation Studies," AIAA Paper 2008-6919, Jun. 2008. https://doi.org/10.2514/6.2008-6919
- [30] Lacy, D. S., and Sclafani, A. J., "Development of the High Lift Common Research Model (HL-CRM): A Representative High Lift Configuration for Transonic Transports," AIAA Paper 2016-0308, Jan. 2016. https://doi.org/10.2514/6.2016-0308
- [31] Hosseini, S.S., van Dam, C.P., and Pandya, S.A., "Aerodynamic Assessment of Surface-Normal Active Flow Control for Lift Enhancement on the High-Lift Common Research Model," AIAA Paper 2023-0433, Jan. 2023. https://doi.org/10.2514/6.2023-0433

- [32] Hosseini, S.S., van Dam, C.P., and Pandya, S.A., "Surface-Normal Active Flow Control for Lift Enhancement and Separation Mitigation for High-Lift Common Research Model," AIAA Paper 2021-1192, Jan. 2021. https://doi.org/10.2514/6.2021-1192
- [33] Anon., "3rd AIAA CFD High Lift Prediction Workshop (HiLiftPW-3)." (https://hiliftpw.larc.nasa.gov/indexworkshop3.html accessed on December 5, 2023)
- [34] Meakin, R., "Object X-rays for Cutting Holes in Composite Overset Structured Grids," AIAA Paper 2001-2537, Jun. 2001. https://doi.org/10.2514/6.2001-2537
- [35] Vassberg, J.C., DeHaan, M.A., Rivers, M.S., and Wahls, R.A., "Retrospective on the Common Research Model for Computational Fluid Dynamics Validation Studies," *Journal of Aircraft*, Vol. 55, No. 4, 2018, pp. 1325-1337. https://doi.org/10.2514/1.C034906
- [36] Atinault, O., and Hue, D., "Design of a Vertical Tail for the CRM Configuration," ONERA Technical Report RT1/21960 GMT/DAAP, June 2014. (https://commonresearchmodel.larc.nasa.gov/wp-content/uploads/sites/7/2017/06/ONERA-LRM-CRM-VTP-Design-Report\_compliant.pdf accessed on December 16, 2023).
- [37] Torenbeek, E., Synthesis of Subsonic Airplane Design, Delft University Press, 1982.
- [38] Lin, J.C., Melton, L.P., Hannon, J.A., Andino, M.Y., Koklu, M., Paschal, K.B., and Vatsa, V.N., "Testing of High-Lift Common Research Model with Integrated Active Flow Control," *Journal of Aircraft*, Vol. 57, No. 6, 2020, pp. 1121-1133. https://doi.org/10.2514/1.C035906
- [39] Stohlgren, L.M., "The GTCP331, a 600 hp Auxiliary Power Unit Program," ASME 83-GT-188, 1983. https://doi.org/10.1115/83-gt-188
- [40] Woodhouse, G.D., "Auxiliary Power Unit Evolution–Meeting Tomorrow's Challenges," SAE Paper 932541, Aerotech '93, Costa Mesa, CA, Sep. 1993. https://doi.org/10.4271/932541
- [41] Kozak, D., and Mazuro, P., "Review of Small Gas Turbine Engines and Their Adaptation for Automotive Waste Heat Recovery Systems," *International Journal of Turbomachinery Propulsion and Power*, Vol. 5, No.2, Jun. 2020. https://doi.org/10.3390/ijtpp5020008
- [42] Van Dam, C.P., Los, S.M., Miley, S.J., Roback, V.E., Yip, L.P., Bertelrud, A., and Vijgen, P.M.H.W., "In-Flight Boundary-Layer State Measurements on a High-Lift System: Main Element and Flap," *Journal of Aircraft*, Vol. 34, No. 6, 1997, pp. 757-763. https://doi.org/10.2514/2.2254
- [43] Rumsey, C.L., Slotnick, J.P., and Woeber, C.D., "HLPW-4/GMGW-3: Overview and Workshop Summary," AIAA Paper 2022-3295, Jun. 2022. https://doi.org/10.2514/6.2022-3295
- [44] Green, E.A., "L-1011 Secondary Power Systems: Design and Function," SAE Paper 740466, SAE Air Transportation Meeting, Dallas, TX, Apr-May 1974. https://doi.org/10.4271/740466
- [45] Huang, B.J., Chang, J.M., Wang, C.P., and Petrenko, V.A., "A 1D Analysis of Ejector Performance," International Journal of Refrigeration, Vol. 22, 1999, pp. 354-364. https://doi.org/10.1016/S0140-7007(99)00004-3
- [46] Chen, W., Liu, M., Chong, D., Yan, J., Little, A.B., and Bartosiewicz, "A 1D Model to Predict Ejector Performance at Critical and Sub-Critical Operational Regimes," *International Journal of Refrigeration*, Vol. 36, 2013, pp. 1750-1761. https://doi.org/10.1016/j.ijrefrig.2013.04.009
- [47] Yip, L.P., van Dam, C.P., Whitehead, J.H., Hardin, J.D., Miley, S.J., Potter, R.C., Bertelrud, A., Edge, D.C., and Willard, P.E., "The NASA B737-100 High-Lift Flight Research Programme Measurements and Computations," *Aeronautical Journal*, Vol. 99, Nov. 1995, pp. 372-386. https://doi.org/10.1017/S0001924000028682
- [48] Brooks, T.R., Kenway, G.K.W., and Martins, J.R.R.A., "Benchmark Aerostructural Models for the Study of Transonic Aircraft Wings," AIAA Journal, Vol. 56, No. 7, 2018, pp. 2840-2855. https://doi.org/10.2514/1.J056603
- [49] Meredith, P., "Viscous Phenomena Affecting High-Lift Systems and Suggestions for Future CFD Development," *High-Lift System Aerodynamics*, AGARD CP-515, 1993, pp. 19–1-19–8.
- [50] https://www.kimerius.com/app/download/5781574315/The+GE90+-+An+introduction.pdf. (accessed on May 2, 2024)
- [51] Slingerland, R., "Minimum Unstick Speed Calculation for High-Speed Jet Transport Aircraft," 24th International Congress of Aeronautical Sciences, ICAS Paper 2004-4.9.3, Aug. 2004.
- [52] Yu, J., Wahls, R., Esker, B., Lahey, L., Akiyama, D., Drake, M., and Christensen, D., "Total Technology Readiness Level: Accelerating Technology Readiness for Aircraft Design," AIAA Paper 2021-2454, Aug. 2021. https://doi.org/10.2514/6.2021-2454